Contribution No. 7374 from The Chemical Laboratories,
California Institute of Technology, Pasadena, California 91125

Oxidative and Hydrolytic Decomposition of a Polyanionic Chelating Ligand

Fred C. Anson, Terrence J. Collins,*[1] Robert J. Coots, Stephen L. Gipson, Terry E. Krafft, Bernard D. Santarsiero, and George H. Spies

Received April 3, 1986

Osmium(IV) complexes of the polyanionic chelating (PAC) ligand 1,2-bis(3,5-dichloro-2-hydroxybenzamido)ethane (H_4CHBA-Et), coordinated as a tetradentate tetraanion, cannot be reversibly electrooxidized at room temperature. Electrooxidation of *trans*-Os(η^4-CHBA-Et)(py)$_2$ in the presence of alcohols results in a sequence of oxidation and hydrolysis reactions involving the ethylene unit of the ligand, [η^4-CHBA-Et]$^{4-}$. The sequence involves 15 observable species. The crystal structures of the species derived by dehydrogenation of the ethylene unit and subsequent oxidation of the C=C double bond to the trans 1-(methyl ether)-2-ol species are presented. The C—C bonds of the metallocyclopentane rings of this trans 1-(methyl ether)-2-ol species and a related *trans*-1,2-bis(methyl ether) analogue are cleaved in further steps to give two diastereomeric complexes (trans and cis (α-derived)) with *N*-formyl substituents. The formyl groups are sequentially hydrolyzed to give primary *N*-amido ligand complexes. The crystal structure of the *trans*-bis(primary *N*-amido) complex *trans*-Os(η^2-CHBA)$_2$(*t*-Bupy)$_2$ (H_2CHBA = 3,5-dichloro-2-hydroxybenzamide) is reported. Evidence is presented for the mono- and diprotonation of the primary amido complexes.

Introduction

We are developing new highly oxidized and highly oxidizing inorganic complexes by utilizing oxidation-resistant polyanionic chelating (PAC) ligands.[2] We recently described the preparation of stable complexes of the PAC ligand **2**, which are strong oxidants

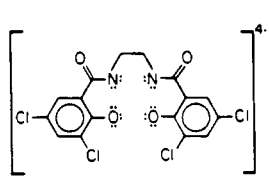

1

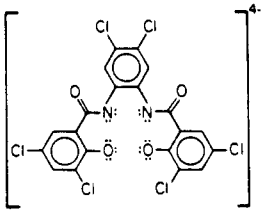

2

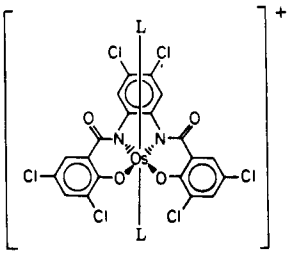

3; L = PPh_3

4; L = py

(1.0–1.4 V vs. SCE), e.g. **3** and **4**.[2a,e] These species were produced by one-electron oxidation of neutral osmium(IV) precursors. However, when electrooxidized in the presence of alcohols, complex **5**, the analogous osmium(IV) complex of PAC ligand **1**, undergoes a sequence of reactions in which the ethylene unit linking the two organic amide nitrogen atoms is degraded by oxidation and hydrolysis. Fifteen of the species in the sequence are observable compounds of which the majority have been isolated and characterized. Six have been characterized by X-ray crystal structure determinations. New complexes that were found to be catalysts for the electrooxidation of alcohols eventually resulted. We recently reported the first steps of the degradation sequence.[2a] Further characterization of the sequence is presented in this paper.

Experimental Section

Materials. All solvents were reagent grade (Aldrich, Baker, Mallinckrodt, MCB or USI) and were used as received unless otherwise noted. Benzyl alcohol (99%, Aldrich), 4-*tert*-butylpyridine (99%, Aldrich), 2,3-dichloro-5,6-dicyano-1,4-benzoquinone (98%, Aldrich), *tert*-butyl alcohol (reagent, Baker), ethanol (absolute, USI), isopropyl alcohol (reagent, Baker), methanol (reagent, Baker), *n*-octanol (99%, Aldrich), hydrogen peroxide (30% Superoxol, Baker), periodic acid (Alfa), pyridine (reagent, Mallinckrodt), tetrabutylammonium hydroxide (25% in methanol, MCB), and triphenylphosphine (99%, Aldrich) were all used as received. Analytical and preparatory thin-layer chromatography plates, 250 and 1000 μm, respectively, were silica gel GF (Analtech).

Syntheses. All reactions were carried out in air unless otherwise noted. $K_2[Os(OH)_4(O)_2]$ was prepared as described in the literature.[3]

3,5-Dichloro-2-hydroxybenzamide (H_2CHBA). Salicylamide (5.00 g) in glacial acetic acid (220 mL) was warmed to 70 °C. Chlorine gas was bubbled through the solution until a yellow color persisted (ca. 0.5 h). The acetic acid was removed under vacuum, and the residue was washed with water and collected by filtration. Recrystallization from acetone/water yielded the product as a white microcrystalline solid: yield 6.98 g (93%); IR (Nujol) 3457 (s, ν_{as}(NH)), 3344 (m, ν_s(NH)), 3215 (br, ν(OH)), 1668 (vs, amide I, ν(CO)), 1620 (s, amide II), 1577 (m), 1259 (s), 1200 (m), 1161 (m), 848 (s), 804 (s), 745 (s) cm^{-1}; ^{1}H NMR (Table I). Anal. Cald for $C_7H_5Cl_2N_1O_2$: C, 40.81; H, 2.45; N, 6.80. Found: C, 40.82; H, 2.53; N, 6.71.

K_2[Os(η^2-CHBA)(O)$_2$]·1.3H_2O (14). Addition of a blue methanol solution of $K_2[Os(OH)_4(O)_2]$ (0.100 g in 25 mL) to a colorless acetone solution containing pure H_2CHBA (0.123 g, 2.2 equiv in 20 mL) produced an immediate color change to deep orange. The solution was stirred at room temperatre for 15 min and then evaporated to dryness to give a quantitative yield of the product. After recrystallization from acetone/CH_2Cl_2 the orange microcrystalline product was dried under vacuum at 80 °C for 7 h. NMR showed the presence of ca. 1.3 molecules of water per molecule of complex: yield 184 mg (93%); IR (Nujol) 1630 (s), 1592 (s), 1565 (s), 1535 (m), 1300 (s), 1235 (s), 1141 (m), 870 (m), 820 (vs. $\nu_{as}(OsO_2)$) cm^{-1}; ^{1}H NMR (Table I). Anal. Calcd for $C_{14}H_6Cl_4K_2N_2O_5Os$·1.3H_2O: C, 22.98, H, 1.18; N, 3.83. Found: C, 22.93; H, 1.16; N, 3.83. Incorporation of ^{18}O was effected by allowing the compound to stand with $H_2{}^{18}O$/acetone for 24 h: IR (Nujol) 788 (vs, $\nu_{as}(Os^{18}O_2)$) cm^{-1}.

(1) Alfred P. Sloan Research Fellow, 1986–1988; Camille and Henry Dreyfus Teacher-Scholar, 1985–1989.

(2) (a) Anson, F. C.; Christie, J. A.; Collins, T. J.; Coots, R. J.; Furutani, T. T.; Gipson, S. L.; Keech, J. T.; Krafft, T. E.; Santarsiero, B. D.; Spies, G. H. *J. Am. Chem. Soc.* **1984**, *106*, 4460–4472. (b) Christie, J. A.; Collins, T. J.; Krafft, T. E.; Santarsiero, B. D.; Spies, G. H. *J. Chem. Soc., Chem. Commun.* **1984**, 198–200. (c) Collins, T. J.; Santarsiero, B. D.; Spies, G. H. *J. Chem. Soc., Chem. Commun.* **1983**, 681–682. (d) Anson, F. C.; Collins, T. J.; Coots, R. J.; Gipson, S. L.; Richmond, T. G. *J. Am. Chem. Soc.* **1984**, *106*, 5037–5038. (e) Anson, F. C.; Collins, T. J.; Gipson, S. L.; Keech, J. T.; Krafft, T. E.; Peake, G. T. *J. Am. Chem. Soc.* **1986**, *108*, 6593–6605. (f) Collins, T. J.; Coots, R. J.; Furutani, T. T.; Keech, J. T.; Peake, G. T.; Santarsiero, B. D. *J. Am. Chem. Soc.* **1986**, *108*, 5333–5339. (g) Barner, C. J.; Collins, T. J.; Mapes, B. E.; Santarsiero, B. D. *Inorg. Chem.* **1986**, *25*, 4322–4323. (h) Anson, F. C.; Collins, T. J.; Gipson, S. L.; Kraft, T. E. *Inorg. Chem.*, in press.

(3) Malin, J. M. *Inorg. Synth.* **1980**, *20*, 61.

0020-1669/87/1326-1161$01.50/0

Table I. 90-MHz ^{1}H NMR Data for Osmium Complexes of $[\eta^2\text{-CHBA}]^{2-}$ [a]

	chem shift, δ					
	chelate ligand		pyridine			
compd	H_1 (amido)	H_2, H_3 (aromatic)[b]	H_o	H_m	*t*-Bu	other
H_2CHBA[c]	13.72 (s, 2 H, br)	7.87 (d, 2 H) 7.40 (d, 2 H)				
14[c]	9.50 (s, 2 H, br)	8.08 (d, 2 H) 7.22 (d, 2 H)				3.68 (s, 2 H; H_2O)
11-*t*-Bupy[d]	44.30 (s, 2 H, br)	10.37 (d, 2 H) 8.97 (d, 2 H)	2.17 (d, 4 H; $J_{o,m}$ = 7.5)	9.10 (d, 4 H; $J_{m,o}$ = 7.5)	1.20 (s, 18 H)	
11′-*t*-Bupy[d]	31.70 (s, 2 H, br)	8.62 (d, 2 H) 8.04 (d, 2 H)	0.52 (d, 4 H; $J_{o,m}$ = 7.5)	8.53 (d, 4 H; $J_{m,o}$ = 7.5)	1.19 (s, 18 H)	
17[d,e]	26.64 (s, 2 H, br)	9.32 (d, 2 H) 8.48 (d, 2 H)	−5.95 (d, 2 H; $J_{o,m}$ = 7.5)	8.95 (d, 2 H; $J_{m,o}$ = 7.5)	0.91 (s, 9 H)	7.33–7.95 (m, 15 H Ph_3P=O)
15[d,f]	56.63 (s, 1 H) 41.38 (s, 1 H)	10.11 (d, 1 H) 8.82 (d, 1 H) 8.78 (d, 1 H) 7.15 (d, 1 H)	−0.58 (d, 2 H; $J_{o,m}$ = 7.5)	9.97 (d, 2 H; $J_{m,o}$ = 7.5)	1.80 (s, 9 H)	7.60–8.35 (m, 15 H Ph_3P=O)

[a] The chemical shifts of the paramagnetic osmium(IV) species are slightly concentration dependent. The values reported here are uncorrected. Coupling constants are reported in Hz. [b] $^{2,3}J$ = $^{3,2}J$ = 3 Hz. [c] In acetone-d_6. [d] In $CDCl_3$. [e] In the 500-MHz spectrum, the ortho, meta, and para proton signals of the Ph_3PO ligand are clearly separated and the couplings are observable. The ortho and meta protons are coupled to the phosphorus by 13.0 and 3.5 Hz, respectively. Coupling with the para protons is not observed. Therefore, the ortho signal is a doublet of doublets and the para signal is a triplet (Figure 1). [f] The 500-MHz spectrum shows the same coupling in the Ph_3PO ligand as seen for complex **17**.

Table II. Data Collection and Refinement Information

	7-*t*-Bupy·$^1/_2CH_2Cl_2$	**8*b**·$^1/_4H_2O$	**11′**-*t*-Bupy·$^1/_2H_2O$·C_2H_5OH
formula	$C_{34.5}H_{35}Cl_5N_4O_4Os$	$C_{27}H_{20.5}Cl_4N_4O_{6.25}Os$	$C_{34}H_{39}Cl_4OsN_4O_{5.5}$
fw	979.61	833.00	923.73
space group	$P\bar{1}$	$P\bar{1}$	$P\bar{1}$
a, Å	10.994 (3)	9.959 (2)	10.439 (4)
b, Å	11.998 (3)	12.740 (2)	12.606 (4)
c, Å	15.660 (3)	15.028 (2)	15.136 (3)
α, deg	99.88 (2)	94.16 (1)	96.04 (2)
β, deg	105.19 (2)	76.74 (1)	102.44 (2)
γ, deg	95.82 (2)	63.48 (1)	101.09 (2)
V, Å^3	1940.5 (8)	1626.8 (5)	1886.3 (9)
Z	2	2	2
D_{calcd}, g cm^{-3}	1.520	1.700	1.643
μ, mm^{-1}	3.396	4.370	3.714
scan type	θ–2θ	θ–2θ	θ–2θ
2θ limits, deg	4–45	4–50	4–40
scan rate, deg/min	2	4	2
scan width, deg	2	1.6	2
tot. no. of collcd reflcns	5583	20518	3910
final no. of reflcns	5092	9048	3531
final no. of params	451	383	406
final cycle[a]			
R_F	0.045 (4083)	0.100 (7694)	0.046 (3406)
R'_F	0.034 (3660)	0.072 (5690)	0.036 (2897)
S	1.81 (5092)	2.14 (9048)	2.39 (3531)

[a] The number of contributing reflections is given in parentheses.

***trans*-Os(η^2-CHBA)$_2$(*t*-Bupy)$_2$ (11′-*t*-Bupy).** $K_2[Os(\eta^2\text{-CHBA})_2(O)_2]\cdot 1.3H_2O$ (**14**) (0.1 g) was dissolved in H_2O (10 mL) and treated with triphenylphosphine (0.085 g, 2.5 equiv) in *tert*-butylpyridine (1.5 mL). The inhomogeneous mixture was stirred at room temperature for 20 min, which produced a color change to deep red-orange. THF (ca. 15 mL) was added, and the resultant homogeneous solution was cooled to 0 °C. After slow addition of H_2O_2 at 0 °C, the reaction mixture was stirred at room temperature for an additional 20 min. The THF was removed by evaporation, which yielded a two-phase mixture. The organic phase was separated, dried over $MgSO_4$, filtered, and evaporated to dryness. Removal of excess *tert*-butylpyridine required heating under vacuum. The residue was dissolved in a minimum of dichloromethane, placed on a silica gel column, and separated by elution with acetone/CH_2Cl_2. The first fraction (blue) contained compound **16**, the second fraction (red), compound **15**, and the last fraction (blue), the desired product, **11′**-*t*-Bupy, which was isolated as a dark blue powder, yield 68 mg (29%). An analytical sample was obtained by purification on a preparatory TLC plate (acetone/hexanes, 3:2) followed by recrystallization from CH_2Cl_2/hexanes: IR (Nujol) 1618 (s, ν(C=O)), 1598 (s), 1578 (m), 1535 (m), 1502 (m), 1289 (s), 1142 (m), 1067 (m, *t*-Bupy), 1040 (m, *t*-Bupy), 874 (m), 843 (m), 801 (m) cm^{-1}; ^{1}H NMR (Table I). Anal. Calcd for $C_{32}H_{32}Cl_4N_4O_4Os$: C, 44.25; H, 3.71; N, 6.45. Found: C, 44.13; H, 3.68; N, 6.31.

***trans*-[Os(η^2-CHBA)$_2$(*t*-Bupy)(Ph_3PO)]·0.15H_2O (17).** Orange $K_2[Os(\eta^2\text{-CHBA})_2(O)_2]_2$ (**14**) (0.425 g) was dissolved in H_2O (40 mL) and treated with triphenylphosphine (0.290 g, 2 equiv) in *tert*-butylpyridine (4 mL) as described above for the synthesis of **11′**. The reduced intermediate was oxidized with H_2O_2 (15 mL), and the product mixture was handled according to the procedure employed for **11′**-*t*-Bupy. The column separation was effected by first eluting with dichloromethane and then gradually increasing the acetone content of the eluent. The first fraction contained compound **15**, and the second yielded **17** as a dark blue powder, yield 233 mg (42%). An analytical sample was obtained by purification on a preparatory TLC plate (acetone/hexane, 3:2) followed by recrystallization from CH_2Cl_2/hexane: IR (Nujol) 1627 (s, ν(C=O)), 1590 (s), 1573 (s), 1530 (m), 1500 (w), 1288 (s), 1125 (s, ν(P=O)), 1080 (m, Ph_3P=O), 1060 (m, *t*-Bupy), 1025 (m, *t*-Bupy), 724 (m, Ph_3P=O) cm^{-1}; ^{1}H NMR (Table I, Figure 1). Anal. Calcd for $C_{41}H_{34}Cl_4N_4O_5OsP\cdot 0.15H_2O$ (solvate quantified by ^{1}H NMR): C, 48.67; H, 3.39; N, 4.15. Found: C, 48.54; H, 3.41; N, 4.14.

***cis*-Os(η^2-CHBA)$_2$(*t*-Bupy)(Ph_3PO) (15).** Compound **14** was formed as a side product in the above synthesis of **11′**-*t*-Bupy and **17**. The yield was variable (10–30%) and was not optimized. The initial column separation of the product mixtures yielded a red fraction that contained **15**. This fraction also contained a significant quantity of organic impurities, and removal of solvents produced a red oil. The oil was converted to a

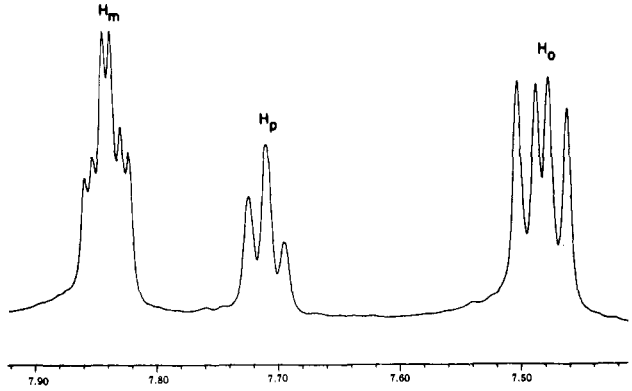

Figure 1. Triphenylphosphine oxide signals in the 500-MHz ^{1}H NMR spectrum of *trans*-Os(η^2-CHBA)$_2$(*t*-Bupy)(Ph$_3$PO) (**17**) (see footnote *e* in Table I).

red powder by vigorous stirring with hexane. The compound was then purified by two successive silica gel columns, each followed by recrystallization from CH_2Cl_2/hexanes. An analytical sample was obtained by further purification on two successive preparatory TLC plates (acetone/hexanes, 3:2) followed by slow crystallization from CH_2Cl_2/hexane and drying under vacuum at 80 °C for 18 h: IR (Nujol) 1615 (s, ν(C=O)), 1598 (sh), 1576 (s), 1536 (m), 1502 (w), 1282 (s), 1122 (s, ν(P=O)), 1066 (s, Ph_3PO), 1023 (m, *t*-Bupy), 725 (m, Ph_3PO) cm^{-1}; ^{1}H NMR (Table I). The analysis results indicate the presence of residual water of solvation that could not be removed with painstaking drying procedures. Analysis was attempted five times for this compound and for the previous compound, **17**. While water of solvation could be observed to disappear with drying to a constant value of 0.15 mol above background in the ^{1}H NMR spectrum of **17**, the presence of the *tert*-butyl signal for **15** obscures the water signal region and prevents quantification of any residual water. Anal. Calcd for $C_{41}H_{34}Cl_4N_3O_5Os$: C, 48.67; H, 3.39; N, 4.15. Found: C, 48.16; H, 3.40; N, 4.21.

***cis*-(α-derived)-Os(η^2-CHBA)$_2$(*t*-Bupy)$_2$ (11-*t*-Bupy).** Compound **5** was oxidized to **9** or **9′** as described above. The anolyte solution containing **9**/**9′**, alcohol, TBAP, and the acid generated during the oxidation process was heated under reflux for 24 h or until TLC indicated that the conversion to **11-*t*-Bupy**/**11′-*t*-Bupy** was complete. The reaction mixture was neutralized. The electrolyte was precipated by addition of ether and was removed by filtration. The filtrate was evaporated to dryness and was redissolved in acetone. The neutral product was precipated by addition of water. The crude product, **11**-*t*-Bupy, was purified on two successive silica gel columns by elution with CH_2Cl_2/acetone and was then recrystallized from CH_2Cl_2/hexanes: IR (Nujol) 1620 (vs, ν(C=O)), 1580 (s), 1538 (m), 1502 (m), 1277 (s), 1137 (m), 1068 (m, *t*-Bupy), 1034 (m, *t*-Bupy), 868 (m), 836 (m), 785 (m) cm^{-1}; ^{1}H NMR (Table I). Anal. Calcd for $C_{32}H_{32}Cl_4N_4O_4Os$: C, 44.25; H, 3.71; N, 6.45. Found: C, 43.94; H, 3.66; N, 6.33.

***cis*-(α-derived)-[Os(η^2-HCHBA)$_2$(py)$_2$](ClO$_4$)$_2$[6] (13).** The unprotonated compound, **11**, was generated by electrolysis and hydrolysis as described above. the reaction mixture was evaporated to dryness and the residue containing the protonated product (ca. 80 mg) and THAP (ca. 2.3 g) was then stirred with benzene (ca. 250 mL) for 15 min. The mixture, which contained the product as a blue oil, was allowed to stand for 2 h and was then decanted. The oily blue solid was washed with a second aliquot of benzene, which was decanted after the mixture stood for 3 h. The blue solid was collected by filtration, dissolved in CH_2Cl_2/acetone, and precipated with hexane. The crystalline product (which was difficult to dry and to obtain free of water of crystallization) was dried under vacuum for 16 h at 80 °C: yield 60 mg; IR (Nujol) 1613 (m, py), 1590 (sh), 1578 (vs), 1535 (sh), 1520 (s), 1153 (vs, ClO_4), 1108 (vs, ClO_4). Anal. Calcd for $C_{24}H_{18}Cl_6N_4O_{12}Os$: C, 30.11; H, 1.90; N, 5.85; Cl, 22.22. Found: C, 30.57; H, 2.21; N, 5.88; Cl, 22.09.

Physical Measurements. ^{1}H NMR spectra were measured at 90 MHz on a Varian EM 390 or a JEOL FX-90Q spectrometer. ^{1}H chemical shifts are reported in δ vs. Me_4Si with the solvent ($CDCl_3$, δ = 7.25; CD_2Cl_2, δ = 5.35; acetone-d_6, δ = 2.05) as internal standard. Infrared spectra were taken as Nujol mulls on KBr windows and were recorded on a Beckman IR 4240 spectrophotometer unless otherwise noted. UV/vis spectra were recorded on a Hewlett-Packard 8450A diode array spectrophotometer. Elemental analyses were obtained at the Caltech Analytical Facility.

Electrochemical Procedures. Dichloromethane (MCB or Mallinckrodt) used in electrochemical experiments was reagent grade and was

Table III. Bond Lengths (Å) and Angles (deg) for *trans*-Os(η^4-CHBA-ethylene)(*t*-Bupy)$_2$ (7-*t*-Bupy)

Os–O(1A)	2.020 (7)	Os–O(1B)	2.011 (8)
Os–N(1A)	1.953 (10)	Os–N(1B)	1.987 (10)
Os–N(2A)	2.072 (9)	Os–N(2B)	2.063 (10)
Cl(1A)–C(5A)	1.762 (14)	Cl(1B)–C(5B)	1.753 (15)
Cl(2A)–C(7A)	1.703 (13)	Cl(2B)–C(7B)	1.718 (13)
Cl(3)–C(18)	1.655 (23)	Cl(4)–C(18)	1.628 (23)
O(1A)–C(8A)	1.340 (14)	O(1B)–C(8B)	1.311 (14)
O(2A)–C(2A)	1.195 (16)	O(2B)–C(2B)	1.211 (17)
N(1A)–C(1A)	1.425 (16)	N(1B)–C(1B)	1.380 (16)
N(1A)–C(2A)	1.415 (16)	N(1B)–C(2B)	1.393 (17)
N(2A)–C(9A)	1.333 (16)	N(2B)–C(9B)	1.308 (15)
N(2A)–C(13A)	1.371 (15)	N(2B)–C(13B)	1.363 (16)
C(1A)–C(1B)	1.346 (17)		
C(2A)–C(3A)	1.496 (17)	C(2B)–C(3B)	1.519 (18)
C(3A)–C(4A)	1.429 (17)	C(3B)–C(4B)	1.405 (18)
C(3A)–C(8A)	1.425 (17)	C(3B)–C(8B)	1.384 (17)
C(4A)–C(5A)	1.383 (18)	C(4B)–C(5B)	1.320 (19)
C(5A)–C(6A)	1.364 (18)	C(5B)–C(6B)	1.415 (20)
C(6A)–C(7A)	1.373 (18)	C(6B)–C(7B)	1.356 (19)
C(7A)–C(8A)	1.432 (17)	C(7B)–C(8B)	1.426 (17)
C(9A)–C(10A)	1.379 (18)	C(9B)–C(10B)	1.400 (17)
C(10A)–C(11A)	1.409 (17)	C(10B)–C(11B)	1.404 (18)
C(11A)–C(12A)	1.363 (18)	C(11B)–C(12B)	1.363 (18)
C(11A)–C(14A)	1.502 (19)	C(11B)–C(14B)	1.491 (21)
C(12A)–C(13A)	1.364 (17)	C(12B)–C(13B)	1.373 (19)
C(14A)–C(15A)	1.425 (35)	C(14B)–C(15B)	1.436 (32)
C(14A)–C(16A)	1.383 (31)	C(14B)–C(16B)	1.401 (32)
C(14A)–C(17A)	1.399 (31)	C(14B)–C(17B)	1.420 (35)
O(1A)–Os–O(1B)	89.1 (3)		
O(1A)–Os–N(1A)	95.3 (4)	O(1A)–Os–N(1B)	76.1 (4)
O(1A)–Os–N(2A)	86.7 (3)	O(1A)–Os–N(2B)	86.8 (3)
O(1B)–Os–N(1A)	75.5 (4)	O(1B)–Os–N(1B)	94.8 (4)
O(1B)–Os–N(2A)	87.9 (3)	O(1B)–Os–N(2B)	87.2 (3)
N(1A)–Os–N(1B)	80.8 (4)		
N(1A)–Os–N(2A)	91.4 (4)	N(1A)–Os–N(2B)	94.0 (4)
N(1B)–Os–N(2A)	93.6 (4)	N(1B)–Os–N(2B)	93.2 (4)
N(2A)–Os–N(2B)	71.9 (4)		
Os–O(1A)–C(8A)	122.5 (7)	Os–O(1B)–C(8B)	123.4 (7)
Os–N(1A)–C(1A)	114.6 (8)	Os–N(1B)–C(1B)	113.6 (8)
Os–N(1A)–C(2A)	129.7 (8)	Os–N(1B)–C(2B)	126.7 (8)
Os–N(2A)–C(9A)	123.2 (8)	Os–N(2B)–C(9B)	121.2 (8)
Os–N(2A)–C(13A)	119.8 (7)	Os–N(2B)–C(13B)	122.6 (8)
C(2A)–N(1A)–C(1A)	115.7 (10)	C(2B)–N(1B)–C(1B)	119.8 (10)
C(13A)–N(2A)–C(9A)	117.0 (10)	C(13B)–N(2B)–C(9B)	116.0 (10)
C(1B)–C(1A)–N(1A)	114.0 (11)	C(1A)–C(1B)–N(1B)	117.0 (11)
N(1A)–C(2A)–O(2A)	122.9 (12)	N(1B)–C(2B)–O(2B)	119.3 (12)
C(3A)–C(2A)–O(2A)	121.3 (11)	C(3B)–C(2B)–O(2B)	120.9 (12)
C(3A)–C(2A)–N(1A)	115.8 (10)	C(3B)–C(2B)–N(1B)	119.7 (11)
C(4A)–C(3A)–C(2A)	111.2 (10)	C(4B)–C(3B)–C(2B)	113.0 (11)
C(8A)–C(3A)–C(2A)	130.0 (11)	C(8B)–C(3B)–C(2B)	126.3 (11)
C(8A)–C(3A)–C(4A)	118.8 (11)	C(8B)–C(3B)–C(4B)	120.7 (11)
C(5A)–C(4A)–C(3A)	118.7 (11)	C(5B)–C(4B)–C(3B)	121.9 (12)
C(4A)–C(5A)–Cl(1A)	118.6 (10)	C(4B)–C(5B)–Cl(1B)	120.3 (11)
C(6A)–C(5A)–Cl(1A)	118.0 (10)	C(6B)–C(5B)–Cl(1B)	119.5 (11)
C(6A)–C(5A)–C(4A)	123.4 (12)	C(6B)–C(5B)–C(4B)	120.2 (13)
C(7A)–C(6A)–C(5A)	119.5 (12)	C(7B)–C(6B)–C(5B)	118.0 (12)
C(6A)–C(7A)–Cl(2A)	121.1 (10)	C(6B)–C(7B)–Cl(2B)	118.0 (10)
C(8A)–C(7A)–Cl(2A)	118.1 (9)	C(8B)–C(7B)–Cl(2B)	118.5 (9)
C(8A)–C(7A)–C(6A)	120.9 (11)	C(8B)–C(7B)–C(6B)	123.6 (12)
C(3A)–C(8A)–O(1A)	126.4 (10)	C(3B)–C(8B)–O(1B)	129.1 (11)
C(7A)–C(8A)–O(1A)	114.9 (10)	C(7B)–C(8B)–O(1B)	115.4 (10)
C(7A)–C(8A)–C(3A)	118.7 (11)	C(7B)–C(8B)–C(3B)	115.6 (11)
C(10A)–C(9A)–N(2A)	121.9 (12)	C(10B)–C(9B)–N(2B)	124.1 (11)
C(11A)–C(10A)–C(9A)	121.9 (12)	C(11B)–C(10B)–C(9B)	119.6 (11)
C(12A)–C(11A)–C(10A)	114.5 (11)	C(12B)–C(11B)–C(10B)	115.6 (12)
C(14A)–C(11A)–C(10A)	122.0 (11)	C(14B)–C(11B)–C(10B)	121.6 (12)
C(14A)–C(11A)–C(12A)	123.5 (12)	C(14B)–C(11B)–C(12B)	122.8 (12)
C(13A)–C(12A)–C(11A)	122.5 (12)	C(13B)–C(12B)–C(11B)	121.6 (12)
C(12A)–C(13A)–N(2A)	122.2 (11)	C(12B)–C(13B)–N(2B)	123.0 (12)
C(15A)–C(14A)–C(11A)	109.3 (16)	C(15B)–C(14B)–C(11B)	113.8 (16)
C(16A)–C(14A)–C(11A)	115.7 (16)	C(16B)–C(14B)–C(11B)	111.8 (16)
C(17A)–C(14A)–C(11A)	112.3 (15)	C(17B)–C(14B)–C(11B)	112.0 (17)
C(16A)–C(14A)–C(15A)	112.7 (20)	C(16B)–C(14B)–C(15B)	102.7 (19)
C(17A)–C(14A)–C(15A)	103.6 (19)	C(17B)–C(14B)–C(15B)	104.4 (20)
C(17A)–C(14A)–C(16A)	102.5 (19)	C(17B)–C(14B)–C(16B)	111.6 (20)
Cl(4)–C(18)–Cl(3)	118.3 (13)		

Scheme I[a]

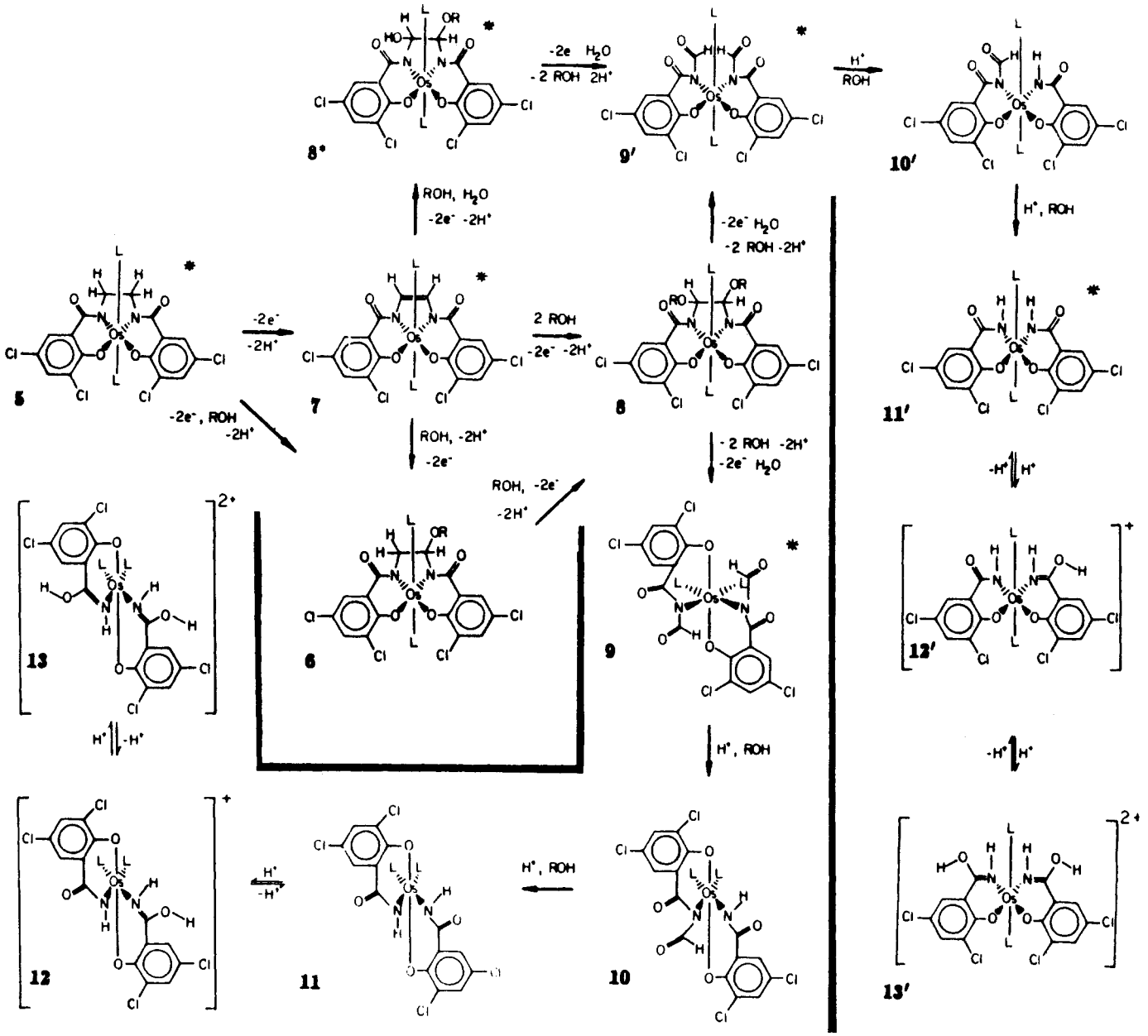

[a] An asterisk denotes a compound characterized by an X-ray crystal structure determination.

further purified by passing it over a column of activated alumina (woelm N. Akt. I). TBAP supporting electrolyte (Southwestern Analytical Chemicals) was dried, recrystallized twice from acetone/ether, and then dried under vacuum. The TBAP concentration in all solutions was 0.1 M. Alcohols were reagent or spectrophotometric grade and were used as received.

Controlled-potential electrolysis experiments were performed with a PAR Model 173 potentiostat equipped with a Model 179 digital coulometer using positive feedback IR compensation. Electrolyses in dichloromethane were performed in a standard three-compartment H-cell with a platinum-gauze counter electrode in one compartment and the reference electrode and a 1.7 × 4.5 × 0.07 cm BPG working electrode in the third compartment. The second compartment separated the other two. The reference electrode used for controlled-potential oxidations with the catalyst compounds was a Corning Ag/AgCl double-junction reference electrode. The product solutions containing decomposed catalysts were found to cause the potential of the usual single-junction Ag/AgCl reference electrode to drift by as much as 500 mV. Therefore, the double-junction reference electrode was used to maintain proximity of the reference electrode to the working electrode and minimize *IR* compensation but, at the same time, isolate the reference electrode from the catalyst solution. The inner compartment of the double-junction reference electrode contained an aqueous solution of saturated KCl and AgCl. The outer compartment contained this solution layered over CH_2Cl_2 containing 0.5 M TBAP. This arrangement gave potentials almost identical with those for the single-compartment electrode but was not susceptible to drift during the electrolyses. Most electrolyses were performed in the presence of solid Na_2CO_3, added to neutralize the acid formed by alcohol oxidation. All experiments were performed at room temperature, 22 ± 2 °C.

X-ray Data Collection for and Structure Determination of $7\cdot{}^1/_2CH_2Cl_2$. A crystal (0.037 × 0.095 × 0.238 mm) of Os(η^4-CHBA-ethylene)(*t*-Bupy)$_2\cdot{}^1/_2CH_2Cl_2$ was obtained by slow crystallization from CH_2Cl_2/hexanes of material isolated from the electrooxidation sequence. Oscillation and Weissenberg photographs indicated no symmetry, and the space group was assumed to be triclinic. The intensity data were collected on a locally modified Syntex $P2_1$ diffractometer with Mo Kα radiation (λ = 0.7107 Å). The unit cell parameters were obtained by least-squares refinement of the orientation matrix using 15 reflections. Three check reflections, remeasured after each block of 97 reflections, indicated a linear decay of less than 1% over the 204 h of data collection. The total number of data (averaged over $\bar{1}$ symmetry) was 5092, of which 3660 had intensities greater than 3σ. The details of the data collection are summarized in Table II.

The atom coordinates of the osmium atom were derived from the Patterson map. Subsequent electron density maps revealed all non-hydrogen atoms. The refinement was carried out as indicated above; the anomalous dispersion factors for osmium and chlorine were included. A

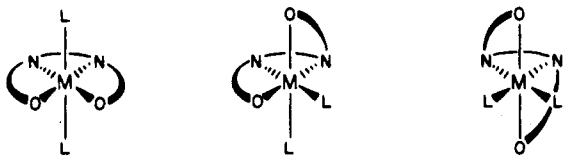

Figure 2. Diastereomeric ligand complements for octahedral complex of tetradentate ligand and two identical monodentate ligands.[7]

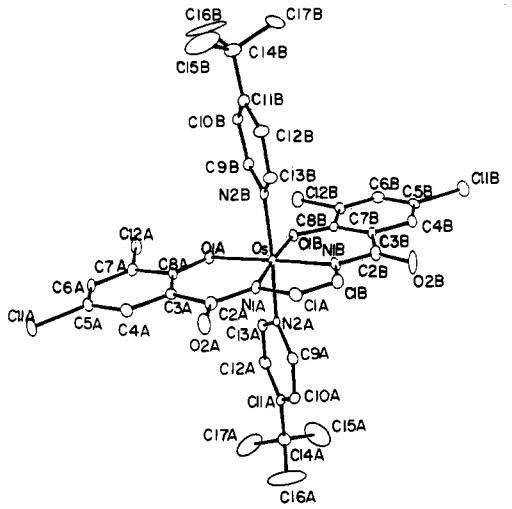

Figure 3. Molecular structure of *trans*-Os(η^4-CHBA-ethylene)(*t*-Bupy)$_2$ (7-*t*-Bupy).

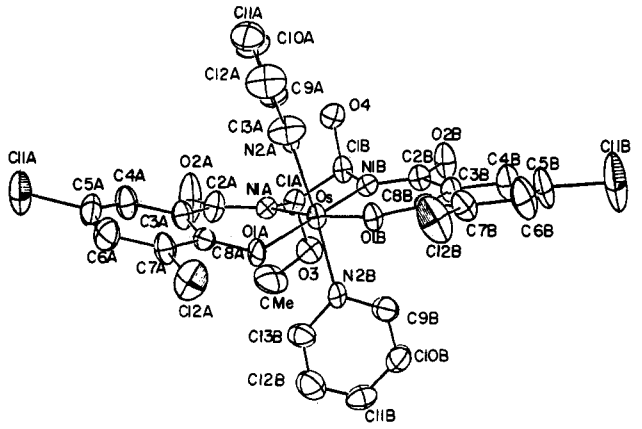

Figure 4. Molecular structure of *trans*-Os(η^4-CHBA-*t*-1-OH-2-OMe-Et)(py)$_2$ (**8*b**).

difference map, calculated after all non-hydrogen atoms had been located, revealed the dichloromethane solvate. At this stage, hydrogen atoms were placed at a distance of 0.95 Å from their respective carbon or oxygen atoms by assuming ideal geometry and were not refined. The hydrogen atoms were given isotropic Gaussian amplitudes of 5.0 Å^2, except for methyl and solvent hydrogen atoms, which were given Gaussian amplitudes of B = 8.0 Å^2.

Final least-squares refinement yielded R_F = 0.072, $R_{3\sigma}$ = 0.050, and S = 1.41;[4] final shift/errors < 0.10; data-to-parameter ratio = 11.3.[5a]

X-ray Data Collection for and Structure Determination of 8*.^{1}/$_4$H$_2$O. A dark blue crystal (0.1 × 0.2 × 0.4 mm) was mounted on a glass fiber. Oscillation and Weissenberg photographs indicated no symmetry; the space group $P\bar{1}$ was assumed. The intensity data were collected on an

Table IV. Bond Lengths (Å) and Angles (deg) for *trans*-Os(η^4-CHBA-*t*-1-OH-2-OMe-Et)(py)$_2$ (**8*b**)

Os–O(1A)	1.991 (7)	Os–O(1B)	1.973 (7)
Os–N(1A)	1.976 (8)	Os–N(1B)	1.983 (8)
Os–N(2A)	2.084 (8)	Os–N(2B)	2.072 (8)
Cl(1A)–C(5A)	1.742 (12)	Cl(1B)–C(5B)	1.733 (14)
Cl(2A)–C(7A)	1.747 (11)	Cl(2B)–C(7B)	1.722 (12)
O(1A)–C(8A)	1.305 (12)	O(1B)–C(8B)	1.310 (12)
O(2A)–C(2A)	1.210 (15)	O(2B)–C(2B)	1.264 (13)
O(3)–C(1A)	1.422 (13)	O(4)–C(1B)	1.389 (12)
O(3)–C(Me)	1.401 (17)		
N(1A)–C(1A)	1.460 (13)	N(1B)–C(1B)	1.477 (13)
N(1A)–C(2A)	1.349 (14)	N(1B)–C(2B)	1.340 (13)
N(2A)–C(9A)	1.340 (14)	N(2B)–C(9B)	1.333 (14)
N(2A)–C(13A)	1.363 (14)	N(2B)–C(13B)	1.323 (14)
C(1A)–C(1B)	1.536 (14)		
C(2A)–C(3A)	1.502 (15)	C(2B)–C(3B)	1.484 (14)
C(3A)–C(4A)	1.409 (16)	C(3B)–C(4B)	1.398 (16)
C(3A)–C(8A)	1.443 (15)	C(3B)–C(8B)	1.450 (14)
C(4A)–C(5A)	1.344 (17)	C(4B)–C(5B)	1.377 (18)
C(5A)–C(6A)	1.366 (17)	C(5B)–C(6B)	1.358 (18)
C(6A)–C(7A)	1.377 (16)	C(6B)–C(7B)	1.392 (17)
C(7A)–C(8A)	1.394 (15)	C(7B)–C(8B)	1.393 (15)
C(9A)–C(10A)	1.367 (18)	C(9B)–C(10B)	1.383 (17)
C(10A)–C(11A)	1.398 (19)	C(10B)–C(11B)	1.343 (18)
C(11A)–C(12A)	1.340 (20)	C(11B)–C(12B)	1.392 (19)
C(12A)–C(13A)	1.310 (19)	C(12B)–C(13B)	1.346 (18)
O(1A)–Os–O(1B)	93.1 (3)		
O(1A)–Os–N(1A)	91.6 (3)	O(1A)–Os–N(1B)	174.3 (3)
O(1A)–Os–N(2A)	83.4 (3)	O(1A)–Os–N(2B)	88.3 (3)
O(1B)–Os–N(1A)	173.6 (3)	O(1B)–Os–N(1B)	92.3 (3)
O(1B)–Os–N(2A)	84.9 (3)	O(1B)–Os–N(2B)	92.5 (3)
N(1A)–Os–N(1B)	83.1 (3)	N(2A)–Os–N(2B)	173.1 (3)
N(1A)–Os–N(2A)	92.1 (3)	N(1A)–Os–N(2B)	92.0 (3)
N(1B)–Os–N(2A)	96.8 (3)	N(1B)–Os–N(2B)	89.7 (3)
Os–O(1A)–O(8A)	122.9 (6)	Os–O(1B)–C(8B)	126.9 (6)
Os–N(1A)–C(1A)	112.3 (6)	Os–N(1B)–C(1B)	114.3 (6)
Os–N(1A)–C(2A)	128.0 (7)	Os–N(1B)–C(2B)	129.2 (7)
Os–N(2A)–C(9A)	125.8 (7)	Os–N(2B)–C(9B)	125.2 (7)
Os–N(2A)–C(13A)	119.3 (7)	Os–N(2B)–C(13B)	121.1 (7)
C(Me)–O(3)–C(1A)	114.2 (9)	O(4)–C(1B)–N(1B)	119.5 (8)
O(3)–C(1A)–N(1A)	112.2 (8)	O(4)–C(1B)–C(1A)	111.3 (8)
O(3)–C(1A)–C(1B)	106.3 (8)		
C(2A)–N(1A)–C(1A)	119.5 (8)	C(2B)–N(1B)–C(1B)	116.3 (8)
C(13A)–N(2A)–C(9A)	114.8 (9)	C(13B)–N(2B)–C(9B)	113.6 (9)
C(1B)–C(1A)–N(1A)	108.9 (8)	C(1A)–C(1B)–N(1B)	107.9 (8)
N(1A)–C(2A)–O(2A)	123.1 (10)	N(1B)–C(2B)–O(2B)	122.4 (9)
C(3A)–C(2A)–O(2A)	118.2 (10)	C(3B)–C(2B)–O(2B)	117.2 (9)
C(3A)–C(2A)–N(1A)	118.7 (9)	C(3B)–C(2B)–N(1B)	120.4 (9)
C(4A)–C(3A)–C(2A)	116.4 (10)	C(4B)–C(3B)–C(2B)	115.9 (9)
C(8A)–C(3A)–C(2A)	125.2 (9)	C(8B)–C(3B)–C(2B)	124.8 (9)
C(8A)–C(3A)–C(4A)	118.3 (9)	C(8B)–C(3B)–C(4B)	119.1 (9)
C(5A)–C(4A)–C(3A)	121.7 (11)	C(5B)–C(4B)–C(3B)	120.7 (11)
C(4A)–C(5A)–Cl(1A)	120.0 (9)	C(4B)–C(5B)–Cl(1B)	119.6 (10)
C(6A)–C(5A)–Cl(1A)	118.3 (9)	C(6B)–C(5B)–Cl(1B)	118.9 (10)
C(6A)–C(5A)–C(4A)	121.6 (11)	C(6B)–C(5B)–C(4B)	121.4 (12)
C(7A)–C(6A)–C(5A)	118.4 (11)	C(7B)–C(6B)–C(5B)	119.0 (12)
C(6A)–C(7A)–Cl(2A)	118.8 (9)	C(6B)–C(7B)–Cl(2B)	118.8 (9)
C(8A)–C(7A)–Cl(2A)	117.4 (8)	C(8B)–C(7B)–Cl(2B)	118.2 (8)
C(8A)–C(7A)–C(6A)	123.7 (10)	C(8B)–C(7B)–C(6B)	122.9 (11)
C(3A)–C(8A)–O(1A)	124.7 (9)	C(3B)–C(8B)–O(1B)	125.3 (9)
C(7A)–C(8A)–O(1A)	119.0 (9)	C(7B)–C(8B)–O(1B)	118.3 (9)
C(7A)–C(8A)–C(3A)	116.2 (9)	C(7B)–C(8B)–C(3B)	116.4 (9)
C(10A)–C(9A)–N(2A)	122.3 (11)	C(10B)–C(9B)–N(2B)	125.7 (11)
C(11A)–C(10A)–C(9A)	120.2 (12)	C(11B)–C(10B)–C(9B)	118.5 (12)
C(12A)–C(11A)–C(10A)	116.6 (13)	C(12B)–C(11B)–C(10B)	117.2 (12)
C(13A)–C(12A)–C(11A)	121.0 (13)	C(13B)–C(12B)–C(11B)	119.6 (12)
C(12A)–C(13A)–N(2A)	125.1 (12)	C(12B)–C(13B)–N(2B)	125.3 (11)

(4) The goodness-of-fit $S = [\sum w\Delta^2/(n-v)]^{1/2}$, n = number of reflections, v = number of parameters, $\Delta = F_o^2 - (F_c^2/k)$; $R_F = \sum|\Delta F|/\sum|F_o|$ (based on reflections with $I > 0$), $\Delta F = |F_o| - |F_c/k|$. $R_{3\sigma} = R_F$ (based on reflections with $I > 3\sigma(I)$).

(5) (a) The CRYM computing system was used (Duchamp, D. J.; Trus, B. L.; Westphal, B. J., California Institute of Technology) on either a VAX 11/870 or a VAX 11/750 computer. (b) Weak reflections were scanned at slower speeds such that $\sigma(I)/I$ = 0.02.

(6) Ligand names: 1,2-bis(3,5-dichloro-2-hydroxybenzamido)ethane, H$_4$-CHBA-Et (**1**); 1,2-bis(3,5-dichloro-2-hydroxybenzamido)-4,5-dichlorobenzene, H$_4$-CHBA-DCB (**2**); 1,2-bis(3,5-dichlorohydroxybenzamido)ethylene, H$_4$-CHBA-ethylene; 1,2-bis(3,5-dichlorohydroxybenzamido)-*trans*-1,2-dialkoxyethane, H$_4$-CHBA-*t*-1,2-diRO-Et; 1,2-bis(3,5-dichloro-2-hydroxybenzamido)-*trans*-1-hydroxy-2-alkoxyethane, H$_4$CHBA-*t*-1-OH-2-OR-Et.

(7) Sargeson, A. M.; Searle, G. H. *Nature* (*London*) **1963**, *200*, 356–357.

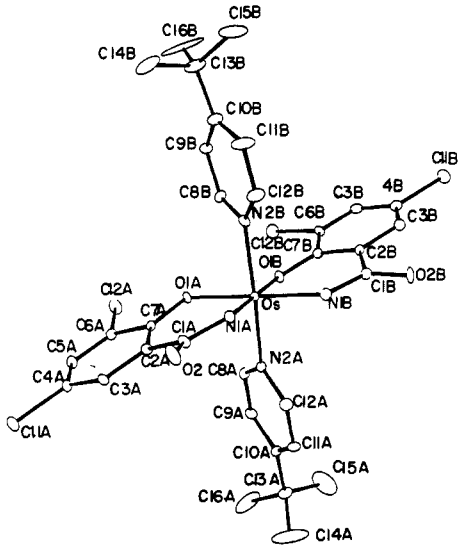

Figure 5. Molecular structure of *trans*-Os(η^2-CHBA)$_2$(*t*-Bupy)$_2$ (**11′-*t*-Bupy**).

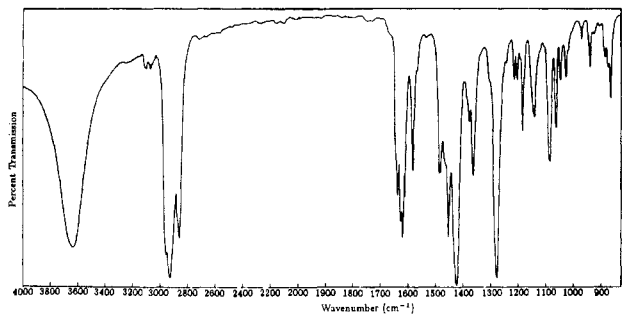

Figure 6. IR spectrum (Nujol mull) of *trans*-Os(η^4-CHBA-ethylene)-(py)$_2$ (**7**) (see footnote 8).

Enraf-Nonius CAD4 diffractometer with Mo Kα radiation (λ = 0.7107 Å) and a graphite monochromator. Lattice parameters were obtained by least-squares refinement of the orientation matrix using 25 centered reflections (19° < 2θ < 40°). The details of data collection are summarized in Table II.

A total of 20518 intensity measurements were recorded for reflections in the entire sphere (2$\theta \leq 50°$) using θ–2θ scans at a speed of 4°/min.[5b] Three check reflections were remeasured after each 10000 s and indicated no decay. No absorption corrections were applied. Averaging of multiple and symmetry related reflections and deletion of several reflections resulted in 9048 average data; 5690 had intensities greater than 3σ.

The position of the osmium atom was derived from a Patterson map, and the subsequent Fourier and difference Fourier maps indicated the location of all non-hydrogen atoms. Hydrogen atoms, except those on the hydroxy and methoxy groups and the uncoordinated water molecule, were placed 0.98 Å from their respective carbon atoms, in idealized positions, and were not refined (B = 4.0 Å^2). The population of the uncoordinated water molecule was set at 0.25.

Several cycles of least-squares refinement led to the final values R_F = 0.100, $R_{3\sigma}$ = 0.072, and S = 2.14.[4] The atom coordinates were in one block, and the scale factor and the Gaussian ellipsoids were in the other.[5a]

X-ray Data Collection for and Structure Determination of 11′-*t*-Bupy. A suitable crystal was obtained by slow crystallization from EtOH/H_2SO_4 of a sample produced from the electrooxidation (Scheme I). Oscillation and Weissenberg photographs showed symmetry no higher than $\bar{1}$. The intensity data were collected on a locally modified Syntex $P2_1$ diffractometer with Mo Kα radiation (λ = 0.7107 Å). The unit cell parameters were obtained by least-squares refinement of the orientation matrix using 15 2θ values. Three standard reflections, remeasured after each block of 197 reflections, indicated a linear decay of ca. 1% over the exposure time of 142 h. The data were corrected for decay and for absorption; averaging gave 3531 reflections, 3406 with $I > 0$ and 2897 with $I > 3\sigma(I)$. The details of data collection are summarized in Table II.

Table V. Bond Lengths (Å) and Angles (deg) for *trans*-Os(η^4-CHBA)$_2$(*t*-Bupy)$_2$ (**11′-*t*-Bupy**)

Os–O(1A)	2.002 (6)	Os–O(1B)	1.993 (6)
Os–N(1A)	1.960 (8)	Os–N(1B)	2.017 (8)
Os–N(2A)	2.089 (8)	Os–N(2B)	2.089 (8)
Cl(1A)–C(4A)	1.743 (10)	Cl(1B)–C(4B)	1.751 (12)
Cl(2A)–C(6A)	1.742 (10)	Cl(2B)–C(6B)	1.732 (11)
O(1A)–C(7A)	1.319 (11)	O(1B)–C(7B)	1.310 (12)
O(2A)–C(1A)	1.240 (13)	O(2B)–C(1B)	1.268 (13)
N(1A)–C(1A)	1.359 (13)	N(1B)–C(1B)	1.330 (14)
N(2A)–C(8A)	1.356 (13)	N(2B)–C(8B)	1.344 (13)
N(2A)–C(12A)	1.353 (14)	N(2B)–C(12B)	1.333 (15)
C(1A)–C(2A)	1.473 (15)	C(1B)–C(2B)	1.480 (15)
C(2A)–C(3A)	1.399 (14)	C(2B)–C(3B)	1.406 (15)
C(2A)–C(7A)	1.427 (14)	C(2B)–C(7B)	1.444 (15)
C(3A)–C(4A)	1.379 (14)	C(3B)–C(4B)	1.370 (16)
C(4A)–C(5A)	1.385 (14)	C(4B)–C(5B)	1.403 (16)
C(5A)–C(6A)	1.349 (14)	C(5B)–C(6B)	1.365 (15)
C(6A)–C(7A)	1.413 (14)	C(6B)–C(7B)	1.385 (15)
C(8A)–C(9A)	1.378 (15)	C(8B)–C(9B)	1.374 (15)
C(9A)–C(10A)	1.380 (15)	C(9B)–C(10B)	1.381 (16)
C(10A)–C(11A)	1.407 (16)	C(10B)–C(11B)	1.391 (18)
C(10A)–C(13A)	1.513 (16)	C(10B)–C(13B)	1.504 (19)
C(11A)–C(12A)	1.374 (16)	C(11B)–C(12B)	1.400 (19)
C(13A)–C(14A)	1.442 (25)	C(13B)–C(14B)	1.502 (25)
C(13A)–C(15A)	1.448 (30)	C(13B)–C(15B)	1.478 (25)
C(13A)–C(16A)	1.460 (24)	C(13B)–C(16B)	1.440 (27)
O(1A)–Os–O(1B)	91.6 (2)		
O(1A)–Os–N(1A)	89.4 (3)	O(1A)–Os–N(1B)	179.2 (3)
O(1A)–Os–N(2A)	87.1 (3)	O(1A)–Os–N(2B)	87.3 (3)
O(1B)–Os–N(1A)	178.7 (3)	O(1B)–Os–N(1B)	88.4 (3)
O(1B)–Os–N(2A)	86.3 (3)	O(1B)–Os–N(2B)	86.6 (3)
N(1A)–Os–N(1B)	90.6 (3)		
N(1A)–Os–N(2A)	94.6 (3)	N(1A)–Os–N(2B)	92.6 (3)
N(1B)–Os–N(2A)	93.7 (3)	N(1B)–Os–N(2B)	91.9 (3)
N(2A)–Os–N(2B)	170.8 (3)		
Os–O(1A)–C(7A)	124.2 (6)	Os–O(1B)–C(7B)	126.9 (6)
Os–N(1A)–C(1A)	129.7 (7)	Os–N(1B)–C(1B)	131.1 (7)
Os–N(2A)–C(8A)	117.3 (6)	Os–N(2B)–C(8B)	118.0 (7)
Os–N(2A)–C(12A)	125.6 (7)	Os–N(2B)–C(12B)	125.1 (7)
C(12A)–N(2A)–C(8A)	116.6 (9)	C(12B)–N(2B)–C(8B)	116.5 (9)
N(1A)–C(1A)–O(2A)	120.1 (10)	N(1B)–C(1B)–O(2B)	123.3 (10)
C(2A)–C(1A)–O(2A)	120.1 (10)	C(2B)–C(1B)–O(2B)	117.5 (9)
C(2A)–C(1A)–N(1A)	119.8 (9)	C(2B)–C(1B)–N(1B)	119.2 (9)
C(3A)–C(2A)–C(1A)	115.2 (9)	C(3B)–C(2B)–C(1B)	115.6 (9)
C(7A)–C(2A)–C(1A)	123.8 (9)	C(7B)–C(2B)–C(1B)	124.7 (9)
C(7A)–C(2A)–C(3A)	120.8 (9)	C(7B)–C(2B)–C(3B)	119.6 (9)
C(4A)–C(3A)–C(2A)	119.7 (9)	C(4B)–C(3B)–C(2B)	119.3 (10)
C(3A)–C(4A)–Cl(1A)	119.5 (8)	C(3B)–C(4B)–Cl(1B)	118.9 (9)
C(5A)–C(4A)–Cl(1A)	119.3 (8)	C(5B)–C(4B)–Cl(1B)	119.0 (9)
C(5A)–C(4A)–C(3A)	121.2 (9)	C(5B)–C(4B)–C(3B)	122.0 (11)
C(6A)–C(5A)–C(4A)	118.7 (9)	C(6B)–C(5B)–C(4B)	118.5 (10)
C(5A)–C(6A)–Cl(2A)	119.0 (8)	C(5B)–C(6B)–Cl(2B)	118.1 (8)
C(7A)–C(6A)–Cl(2A)	116.7 (7)	C(7B)–C(6B)–Cl(2B)	118.8 (8)
C(7A)–C(6A)–C(5A)	124.3 (9)	C(7B)–C(6B)–C(5B)	123.0 (10)
C(2A)–C(7A)–O(1A)	125.5 (9)	C(2B)–C(7B)–O(1B)	124.3 (9)
C(6A)–C(7A)–O(1A)	119.2 (9)	C(6B)–C(7B)–O(1B)	118.2 (9)
C(6A)–C(7A)–C(2A)	115.2 (9)	C(6B)–C(7B)–C(2B)	117.6 (9)
C(9A)–C(8A)–N(2A)	122.7 (9)	C(9B)–C(8B)–N(2B)	123.0 (10)
C(10A)–C(9A)–C(8A)	121.2 (10)	C(10B)–C(9B)–C(8B)	121.9 (10)
C(11A)–C(10A)–C(9A)	115.9 (10)	C(11B)–C(10B)–C(9B)	114.9 (11)
C(13A)–C(10A)–C(9A)	121.7 (10)	C(13B)–C(10B)–C(9B)	122.7 (11)
C(13A)–C(10A)–C(11A)	122.4 (10)	C(13B)–C(10B)–C(11B)	122.4 (11)
C(12A)–C(11A)–C(10A)	120.5 (10)	C(12B)–C(11B)–C(10B)	120.5 (12)
C(11A)–C(12A)–N(2A)	123.1 (10)	C(11B)–C(12B)–N(2B)	123.0 (11)
C(14A)–C(13A)–C(10A)	113.3 (12)	C(14B)–C(13B)–C(10B)	108.1 (12)
C(15A)–C(13A)–C(10A)	107.2 (14)	C(15B)–C(13B)–C(10B)	110.7 (13)
C(16A)–C(13A)–C(10A)	113.4 (12)	C(16B)–C(13B)–C(10B)	112.8 (14)
C(15A)–C(13A)–C(14A)	112.4 (16)	C(15B)–C(13B)–C(14B)	104.4 (14)
C(16A)–C(13A)–C(14A)	101.8 (14)	C(16B)–C(13B)–C(14B)	109.4 (15)
C(16A)–C(13A)–C(15A)	108.8 (16)	C(16B)–C(13B)–C(15B)	111.2 (15)

The position of the osmium atom was derived from a Patterson map, and the subsequent difference Fourier maps indicated the locations of the remaining non-hydrogen atoms of the ligands. The disordered solvent molecules were placed in positions derived from difference Fourier maps. The hydrogen atoms were placed at calculated positions and were not refined. Several cycles of full-matrix least-squares refinement of all

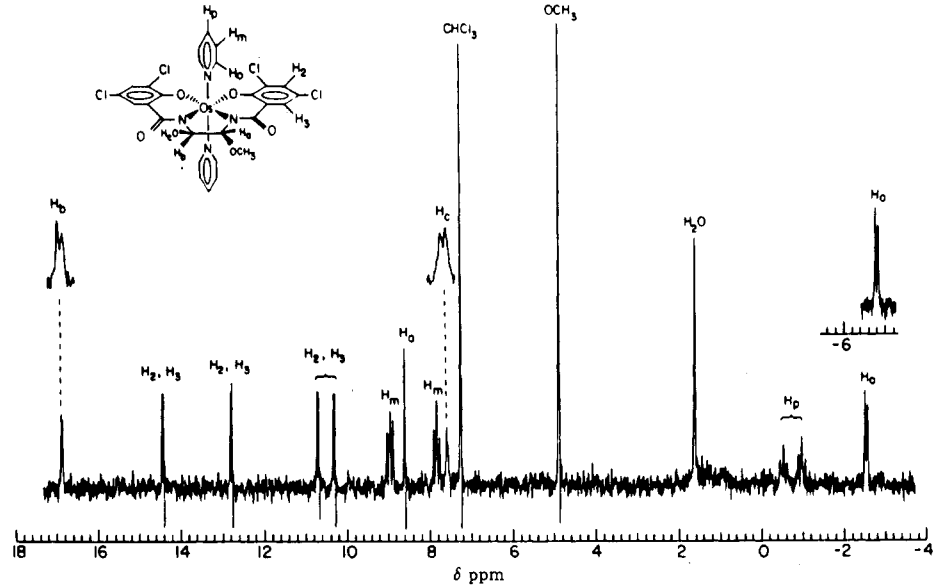

Figure 7. 90-MHz ^{1}H NMR spectrum of *trans*-Os(η^4-CHBA-*t*-1-OH-2-OMe-Et)(py)$_2$ (**8*b**) (see footnote 8).

non-hydrogen parameters yielded $R_F = 0.046$, $R_{3\sigma} = 0.036$, and $S = 2.39$.[4,5]

Results and Discussion

Further Characterization of Intermediates in Oxidation Segment of Degradation Sequence. The observable complexes in the ligand oxidation and hydrolysis sequence are depicted in Scheme I. The progress of the sequence through compounds **5**, **7**, **8**, **8***, **9**, and **9′** has been reported.[2a] Each of these steps involves an oxidation process. In the initial report complexes **7**, **8**, and **8*** were assumed to have trans structures (Figure 2). ^{1}H NMR measurements established C_2 symmetry for **7**[8,11] and **8**, ruling out the cis-β diastereomer, but no direct evidence distinguished the trans or cis-α formulations. Because of the low symmetry of **8***, it was impossible to eliminate any of the three possible diastereomeric forms on the basis of NMR properties. X-ray crystal structures for **7** (L = *t*-Bupy; see Figure 3, Table III) and for **8*** (R = Me; see Figure 4, Table IV) confirm that each has the trans structure. By implication, compound **8** is also a trans diastereomer.

Further Degradation of Complexes 9 and 9′. When **5** is bulk electrolyzed in dichloromethane/alcohol solutions, current is passed until compounds **9** and/or **9′** are formed. If this solution is allowed to stand to rom temperature, TLC reveals that **9** and **9′** slowly undergo further transformations. These processes occur rapidly if the electrolysis solution is heated under reflux. Alternatively, the conversions can be affected by heating **9** or **9′** under reflux in dichloromethane containing alcohol (1 M) and trace quantities of perchloric acid. TLC analysis of the course of these reactions indicates that each of the blue compounds **9** and **9′** degrades in two steps through two separate blue compounds to two final blue compounds. These final compounds, **11** and **11′**, can be isolated. The TLC-detectable intermediates are presumably **10** and **10′**. Poor solubility of the pyridine adducts prompted us to synthesize the more soluble *tert*-butyl pyridine derivatives, which exhibit well-resolved paramagnetically shifted ^{1}H NMR spectra (Table I).

The results of an X-ray crystal structure determination for **11′**-*t*-Bupy) are shown in Figure 5 (Table V). This is the first example of an N-coordinated primary amide complex of osmium(IV). The primary amide hydrogen atoms could not be located due to the proximity of these atoms to the osmium atom and limitations of the structural data. We were concerned that the bidentate ligands might be coordinated via O-bonded oxyimine ligands rather than N-bonded amido ligands as the observed bond lengths and angles are compatible with both formulations. The IR spectrum shows a strong band in the carbonyl region that is consistent with the amide or imine structures. The intensities of bands associated with imine stretches are variable.[12] The chemical properties of **11** and **11′** support the amide formulation. Primary imines are highly susceptible to hydrolysis,[13] but **11** and **11′** are

(8) The IR spectrum of compound **7** contains an unusual feature (Figure 6). A very strong, broad band, present in both the solid and solution spectra, occurs between 3300 and 4000 cm^{-1}. No functional groups are present in **7** that could account for a vibrational mode in this region. The X-ray structure, NMR and elemental analysis data rule out the presence of O–H groups. Other explanations based on vibrational processes are unlikely for a band of this intensity in this position. The band could arise from a low-energy electronic transition (λ_{max} = 2750 nm, $\epsilon \approx 5 \times 10^2$). Electronic transitions in the IR region are rare and have been found for mixed-valence dimers, but are commonly observed at higher energies.[9a-e] The IR spectra of compound **5** also contains an unexplained band in the 3000–4000-cm^{-1} region, and compounds **8**, **8***, **11** and **11′** contain shoulders at 4000 cm^{-1} (the instrument cutoff), which might indicate a generality to this phenomenon for these osmium(IV) species. In these latter cases the bands occur at higher energy than the normal range for ν(OH) activity.[9f,g] A second unusual spectroscopic feature is found for the coupling constants in the ^{1}H NMR spectra of the **8*** compounds. The 90-MHz ^{1}H NMR spectrum of **8*b** is depicted in Figure 7. The asymmetry in **8*b** is clearly evident in this spectrum. Coupling between H_b and H_c indicates that the exchange rate for H_c is slow on the NMR time scale. The absence of observable coupling between H_b and H_a is also unusual and initially led us to doubt the formulation that we subsequently substantiated by crystallography. However, vicinal coupling constants in saturated systems are highly dependent upon the dihedral angle (between the planes containing the nuclei in question and the intervening carbon atoms), θ, with the largest coupling constants being observed for θ = 0 or 180°, and the smallest value being observed for θ = 90°.[10a] In the crystal structure of **8*b**, H_a and H_b are both equatorial and the relevant dihedral angle is close to 90°. Substituent effects can also lower coupling constants and could be important in this case.[10b]

(9) (a) Magneson, R. H.; Lay, P. A.; Taube, H. *J. Am. Chem. Soc.* **1983**, *105*, 2507–2509. (b) Creutz, C.; Taube, H. *Ibid.* **1973**, *95*, 1086–1094. (c) Magneson, R. H.; Taube, H. *Ibid.* **1972**, *94*, 7213–7214. (d) Creutz, C.; Taube, H. *Ibid.* **1969**, *91*, 3988–3989. (e) Richardson, D. E.; Sen, J. P.; Buhr, J. D.; Taube, H. *Inorg. Chem.* **1982**, *21*, 3136–3140. (f) Nakamoto, K. *Infrared and Raman Spectra of Inorganic and Coordination Compounds*; Wiley: New York, 1978; p 111. (g) Silverstein, R. M.; Bassler, G. C.; Morrill, T. C. *Spectrophotometric Identification of Organic Compounds*, 3rd. ed.; Wiley: New York, 1974; pp 91–95.

(10) (a) Karplus, M. *J. Chem. Phys.* **1959**, *30*, 11–15. (b) Reference 9g; pp 174–176.

(11) (a) For a recent review of α,α-diimine complexes, including ligand oxidations, see: Van Koten, G.; Vrieze, K. *Adv. Organomet. Chem.* **1982**, *21*, 151–239. (b) Oxidation of methylene units of N-coordinated organic amido ligands in polypeptide chelating ligand systems has been reported: Rybka, J. S.; Margerum, D. W. *Inorg. Chem.* **1981**, *20*, 1453–1458. Kirschenbaum, L. J.; Rush, J. D. *J. Am. Chem. Soc.* **1984**, *106*, 1003–1010.

(12) Reference 9g; p 111.

(13) March, J. *Advanced Organic Chemistry*, 2nd ed.; McGraw-Hill: New York, 1977; p 806.

Scheme II

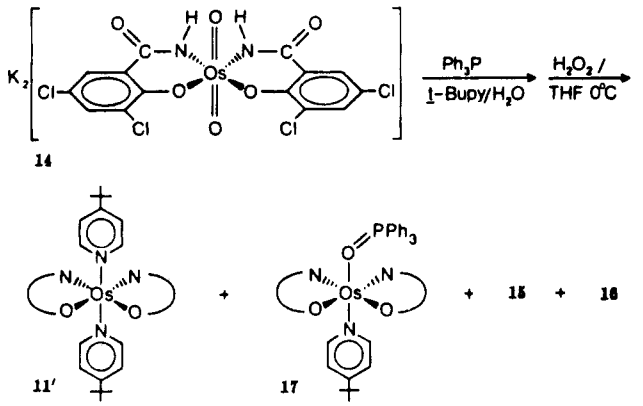

stable in the presence of strong acid. A reexamination of the X-ray data was performed as follows. The structure was refined with appropriate form factors for the amide structure. The atoms in position 1 (atom attached to metal) were assigned a nitrogen form factor and the atoms in position 2 (heteroatom not attached to metal) were assigned an oxygen form factor. This produced reasonable isotropic thermal parameters for the atoms in question (oxygens = 3.98 and 4.35; nitrogens = 2.61 and 3.33). The same data were then refined with the form factors switched, resulting in unsatisfactory isotropic thermal parameters for the four atoms (position 1 = 1.85 and 2.05; position 2 = 5.02 and 5.94). These results further support the amide formulation.

The visible spectrum of the **11′** analogue **17** (vide infra) was monitored during the addition of small aliquots of $HBF_4 \cdot Et_2O$. The experiment indicates the stepwise formation of two species (**17**, λ_{max} = 540 nm, $\epsilon_{540} = 9.24 \times 10^3$ L cm^{-1} mol^{-1}; fully protonated form λ_{max} = 590 nm, $\epsilon_{590} = 7.07 \times 10^3$ L cm^{-1} mol^{-1}). These transformations are fully reversible; addition of base restores the spectrum of the deprotonated complexes. This suggests that **17** can be mono- and diprotonated. Similar results were found for **11** and **11′**. We favor the amide oxygen atoms as the sites of protonation (**12**, **12′**, **13**, and **13′**, Scheme I). O-Protonation of secondary and primary N-coordinated amido ligands has been characterized crystallographically,[14] and a large body of additional evidence supports the O-protonation of N-amido ligands.[15] Complex **13** has been isolated from the electrochemical reaction mixture as a diperchlorate salt. The monoprotonated forms **12** and **12′** could not be isolated as crystalline materials because deprotonated **11** and **11′** crystallize preferentially from weakly acidic solutions. We have presented evidence showing that, of the complexes in Scheme I, only **12**, **12′**, **13**, and **13′** are possible candidates for the catalytically active species in the electrocatalytic oxidation of alcohols.[2h]

(14) (a) Barnet, M. T.; Freeman, H. C.; Buckingham, D. A.; Hsu, I-Nan; van der Helm, D. *J. Chem. Soc. D.* **1970**, 367–368. (b) Sekizaki, M. *Bull. Chem. Soc. Jpn.* **1978**, *51*, 1991–1995.

(15) See for example: (a) Buckingham, D. A.; Forster, D. M.; Sargeson, A. M. *J. Am. Chem. Soc.* **1969**, *91*, 3451–3456. (b) Margerum, D. W. *Pure Appl. Chem.* **1983**, *55*, 23–24. (c) Margerum, D. W.; Cagley, G. R.; Weatherburn, D. C.; Pagenkoph, G. K. *ACS Monogr.* **1978**, *No. 174*, 1–220. (d) Jacobs, S. A.; Margerum, D. W. *Inorg. Chem.* **1984**, *23*, 1195–1201. (e) Raycheba, J. M. T.; Margerum, D. W. *Ibid.* **1980**, *19*, 497–500. (f) Rybka, J. S.; Kurtz, J. L.; Neubecker, T. A.; Margerum, D. W. *Ibid.* **1980**, *19*, 2791–2796. (g) DeKorte, J. M.; Owens, G. D.; Margerum, D. W. *Ibid.* **1979**, *18*, 1538–1542. (h) Cooper, J. C.; Wong, L. F.; Margerum, D. W. *Ibid.* **1978**, *17*, 261–266. (i) Wong, L. F.; Cooper, J. C.; Margerum, D. W. *J. Am. Chem. Soc.* **1976**, *98*, 7268–7274. (j) Paniago, E. B.; Margerum, D. W. *Ibid.* **1972**, *94*, 6704–6710. (k) Hay, R. W.; Mahesh, P. P.; McLaren, F. *Inorg. Chem.* **1984**, *23*, 3033–3035. (l) Nonoyama, M. *Inorg. Chim. Acta* **1975**, *13*, 5–10. (m) Hawkins, C. J; Kelso, M. T. *Inorg. Chem.* **1982**, *21*, 3681–3686. (n) Hodgson, J. B.; Percy, G. C. *J. Mol. Struct.* **1977**, *37*, 193–198. (o) Mogilevkina, M. F.; Smirnov, M. Yu.; Korobeinicheva, I. K.; Senchenko, L. N. *Zh. Neorg. Khim.* **1981**, *26*, 3024–3028; *Chem. Abstr.* **1982**, *96*, 27708f.

Alternative Syntheses of Primary *N*-Amido Complexes. The direct conversion of **5** to the doubly protonated forms of **11** and **11′**, can be carried out in situ without isolation of the intermediate compounds. However, these complicated sequential electrochemical and hydrolytic syntheses were inconvenient. We sought a more direct chemical route to the primary N-amido complexes and discovered that salicylamide bidentate ligands could be directly coordinated to osmium. A blue methanol solution of osmate, $K_2[Os(O)_2(OH)_4]$, was added at room temperature to an acetone solution containing 2 equiv of dichlorosalicylamide. The reaction affords $K_2[Os(\eta^2\text{-CHBA})_2(O)_2]$ (**14**) in quantitative yield as a gold-brown powder (Scheme II). We assume that the doubly deprotonated dichlorosalicylamide is N-coordinated. The relative orientation of the two bidentate ligands of **14**, cis versus trans nitrogens, cannot be deduced directly from the spectroscopic data (IR, ^{1}H NMR), but the cis diastereomer is likely since **11′** can be synthesized directly from **14**.

Reduction of **14** with triphenylphosphine in the presence of *tert*-butylpyridine, followed by oxidation of the reduced products, affords a variable mixture of four components (Scheme II) depending on the conditions. If the reduction is carried out at the same temperature at which **5** is produced (60 °C), then very little of any product can be extracted from the reduced reaction medium. At room temperature the synthesis affords **11′** and two additional compounds, **15** and **16**. At 0 °C a new compound, **17**, is formed in moderate yield with only one side product, **15**. The products can be separated by column and thin-layer chromatography. The maximum yield of **11′**-*t*-Bupy obtained from the room-temperature reaction was 29%. This procedure represents a significant streamlining of the synthesis of **11′**, but no **11** has been obtained from this route. Compound **15** is either one of the two possible cis-α-derived diastereomers or the cis-β-derived diastereomer of compound **17**, but the sectroscopic data (IR, ^{1}H NMR) do not permit the isomers to be distinguished. Both **15** and **17** are similar to **11** and **11′** in that they are converted to catalysts for the electrooxidation of alcohols in the presence of acid. Compound **16** has not been identified at this stage. This species shows some activity for the catalytic electrooxidation of alcohols.

Conclusion

In this report we have described further results on the ligand oxidation and hydrolytic degradation of osmium complexes of the PAC ligand $[\eta^4\text{-CHBA-Et}]^{4-}$. It should be noted that the complexity found in the sequence is associated with stepwise transformations of a simple ethylene group. In a prior report we have described the alcohol electrocatalytic oxidations found for several species in the sequence.[2h]

Acknowledgment. We acknowledge the Rohm and Haas Co. and the Atlantic Richfield Corp. of America for support to T.J.C. and the National Science Foundation (Grants CHE-84-06198 to T.J.C. and CHE-83-11579 to F.C.A.). R.J.C. thanks the Exxon Education Foundation for postdoctoral support. S.L.G. thanks the NSF for a predoctoral fellowship and the IBM Corp. for the award of the Caltech IBM Fellowship. T.E.K. thanks Union Carbide for the award of a Union Carbide Fellowship in Chemical Catalysis. We thank Drs. William P. Schaefer and Richard E. Marsh of this department and Professor Warren Roper of the University of Auckland, New Zealand, for helpful discussions. We thank the Engelhard Corp. for a generous donation of precious metal compounds. Upgrade of the X-ray diffraction facility was supported by NSF Grant CHE-82-19039 to the Division of Chemistry and Chemical Engineering.

Supplementary Material Available: Listings of fractional atomic coordinates and Gaussian amplitudes (10 pages); listings of structure factor amplitudes (76 pages). Ordering information is given on any current masthead page.